The Lag Model Applied to High Speed Flows

Michael E. Olsen *
NASA Ames Research Center
Moffett Field, CA 94035

Randolph P. Lillard †‡
Purdue University
West Lafayette, IN 47907-1282, US

Thomas J. Coakley §
NASA Ames Research Center
Moffett Field, CA 94035

The Lag model has shown great promise in prediction of low speed and transonic separations. The predictions of the model, along with other models (Spalart-Allmaras and Menter SST) are assessed for various high speed flowfields. In addition to skin friction and separation predictions, the prediction of heat transfer are compared among these models, and some fundamental building block flowfields, are investigated.

I. Introduction

One difficulty with current one and two-equation turbulence models is the inability to account directly for non-equilibrium effects such as those encountered in large pressure gradients involving separation and shockwaves. Current turbulence models such as Spalart's one-equation model,[1] the classic $k-\epsilon$ and Wilcox's $k-\omega$[2] two-equation models have been designed and tuned to accurately predict equilibrium flows such as zero-pressure gradient boundary- layers and free shear layers. Application in more complex flows can be problematical at best. Although there have been many attempts to modify or correct basic one- and two-equation models, most of these attempts have been only marginally successful in predicting complex flows.

More complex models such as Reynolds stress models have been investigated extensively, primarily for relatively simple flows but also for complex flows. In most cases these models give somewhat better predictions than the simpler one and two equation models, but for complex flows they do not perform much better than the simpler models. One theoretical advantage of Reynolds stress models is that they directly account for non-equilibrium effects in the sense that the Reynolds stresses do not respond instantaneously to changes to the strain rate but more realistically lag them in time and/or space. Unfortunately, The Reynolds stress models are usually considerably more complicated and numerically stiff than the one- and two- equation models, and this has prevented their wide application for complex flows.

In this paper we further investigate the Lag model, which was designed to account for non-equilibrium effects without invoking the full formalism of the Reynolds stress models. The basic idea is to take a baseline two-equation model and to couple it with a third (lag) equation to model the non-equilibrium effects for the eddy viscosity. The third equation is designed to predict the equilibrium eddy viscosity in equilibrium flows. One advantage of this method over comparable turbulence models is that it does not require wall distance, a major advantage for some flow solvers, and in complex flowfields where wall distance determination is a non-trivial exercise.

Applications to four flows will be given including a high speed flat plate, cylinder flares, a rocket nozzle with significant separation, and space vehicles.

---

*Research Scientist, NASA Ames Research Center, Associate Fellow AIAA
†Research Assistant, Student Member, AIAA
‡Aerospace Engineer, NASA Johnson Space Center, Aerosciences and CFD Branch
§Research Scientist, NASA Ames Research Center, Associate Fellow AIAA

II. Method

A. Reynolds Averaged Navier Stokes Equations

The Reynolds averaged Navier-Stokes equations, written in conservation law form are

$$\frac{\partial Q}{\partial t} + \frac{\partial F_i}{\partial x_i} = 0 \tag{1}$$

Where

$$Q=[\rho,\ \rho u_1,\ \rho u_2,\ \rho u_3,\ \rho\varepsilon_T,] \tag{2}$$

$$F_1=[\rho u_1,\ \rho u_1^2+\tilde{p}+\tau_{11},\ \rho u_1 u_2+\tau_{12},\ \rho u_1 u_3+\tau_{13},\ \rho u_1(\varepsilon_T+\tilde{p}+\tau_{11})+u_2\tau_{12}+u_3\tau_{13}+q_1] \tag{3}$$

$$F_2=[\rho u_2,\ \rho u_2 u_1+\tau_{21},\ \rho u_2^2+\tilde{p}+\tau_{22},\ \rho u_2 u_3+\tau_{23},\ \rho u_2(\varepsilon_T+\tilde{p}+\tau_{22})+u_3\tau_{23}+u_1\tau_{21}+q_2] \tag{4}$$

$$F_3=[\rho u_3,\ \rho u_3 u_1+\tau_{31},\ \rho u_3 u_2+\tau_{32},\ \rho u_3^2+\tilde{p}+\tau_{33},\ \rho u_3(\varepsilon_T+\tilde{p}+\tau_{33})+u_1\tau_{31}+u_2\tau_{32}+q_3] \tag{5}$$

where: $\varepsilon = \int_0^T c_v\,dT = c_v T$ $\quad q_i = \dfrac{(\mu/Pr+\mu_t/Pr_t)}{\gamma}\dfrac{\partial\epsilon}{\partial x_i}$ $\quad \tilde{p} = p+\dfrac{2k}{3}$

$\varepsilon_t = \varepsilon + (u_i u_i)/2 + k$ $\quad p = (\gamma-1)\rho\varepsilon$

Turbulent kinetic energy, k, is simply assumed to be zero for the 1 equation turbulence models.

B. Lag Model, Revised

The Lag model has been revised from the original description.[3] It was simplified from the original description by dropping the leading function of R_T in the lag equation, and the constant defining the diffusion of the underlying k equation(σ_k) was increased to 1.5. This change was cosmetic, in that it rounded the turbulent/non-turbulent edge of the boundary layers and simplified up the model(the leading function of R_T was found to be unnecessary). All cases reported[3] earlier were re-run, and the previous results were reproduced, with minor improvement in the Johnson-Bachalo bump case.

The revised Lag model is

$$\frac{\partial\rho k}{\partial t}+\frac{\partial}{\partial x_i}\left(\rho u_i k-(\mu+\sigma_k\rho\nu_t)\frac{\partial k}{\partial x_i}\right) = \mathcal{P}_k-\epsilon_k \tag{6}$$

$$\frac{\partial\rho\omega}{\partial t}+\frac{\partial}{\partial x_i}\left(\rho u_i\omega-(\mu+\sigma_\omega\rho\nu_t)\frac{\partial\omega}{\partial x_i}\right) = \mathcal{P}_\omega-\epsilon_\omega \tag{7}$$

$$\frac{\partial\rho\nu_t}{\partial t}+\frac{\partial}{\partial x_i}\left(\rho u_i\nu_t\right) = a_0\rho\omega\,(\nu_{t_\varepsilon}-\nu_t) \tag{8}$$

where:

$$\nu_{t_\varepsilon} = k/\omega \qquad \mathcal{P}_\omega = \alpha\rho S^2$$

$$\mathcal{P}_k = \tau_{ij}s_{ij} \qquad \epsilon_\omega = \beta\rho\omega^2$$

$$\epsilon_k = \beta^*\rho k w \qquad S = \sqrt{2\left(s_{ij}s_{ij}-s_{kk}^2/3\right)}$$

$$\tau_{ij} = \rho\left(\frac{2}{3}k\delta_{ij}-\nu_t(2s_{ij}-\frac{2}{3}s_{kk}\delta_{ij})\right) \qquad s_{ij} = \frac{1}{2}\left(\frac{\partial u_i}{\partial x_j}+\frac{\partial u_j}{\partial x_i}\right)$$

with parameters

$$a_0 = 0.35 \qquad \beta = 0.075 \qquad \sigma_k = 1.5$$

$$\alpha = 5/9 \qquad \beta^* = 0.09 \qquad \sigma_e = 0.5$$

C. Numerical Method

The code used in this study was OVERFLOW2, modified to include the Lag model along with the high speed modifications involving the k discussed with the Navier Stokes Equations. Matrix dissipation was used with smoothing parameters as recomended by earlier studies of high speed flows with this code.[4] These values proved suitable for these flows also(Fig1(a),1(b)), in that doubling and halving both second and fourth order smoothing coefficients did not affect the flowfields. The recommended eigenvalue limits ($V_{\epsilon_n} = 0.3, V_{\epsilon_l} = 0.3$) are not adjusted.

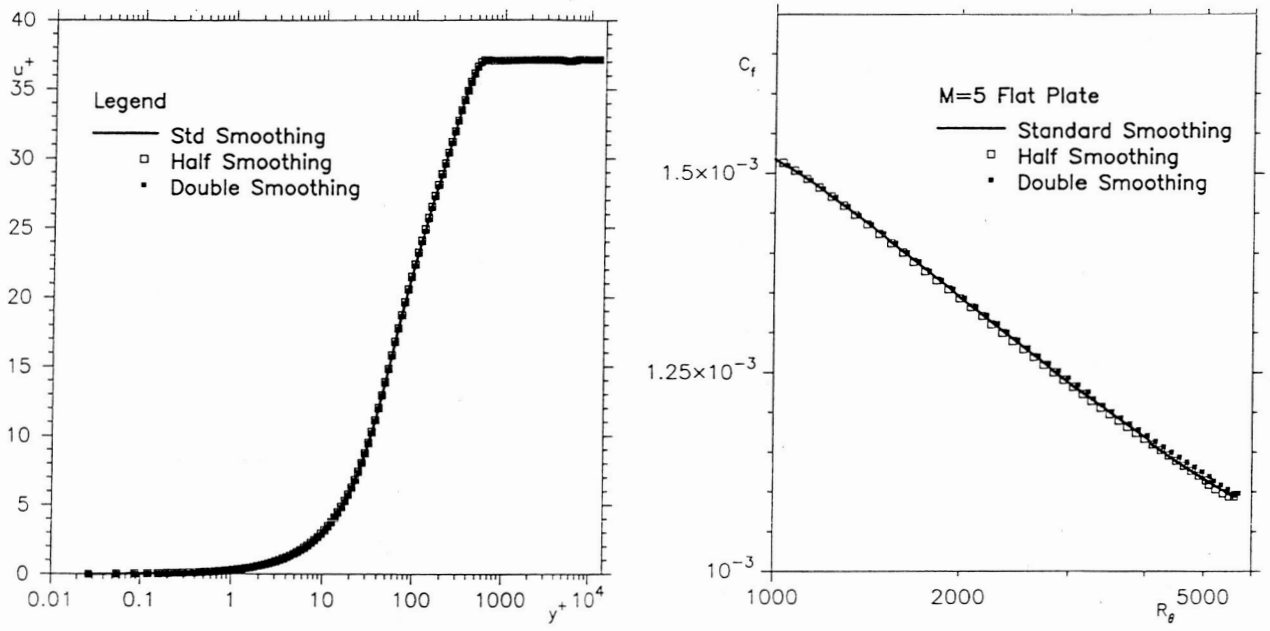

(a) Boundary Layer

(b) Skin Friction,x/L = .1

Figure 1. Insensitivity of Solution to Smoothing Parameters, Flat Plate Solution

The relaxation method is the implicit Pulliam Chausee diagonal method, with variable time stepping(ITIME=1) or constant CFL (itime=3). CFL values for these high speed flows were chosen at 0.4, and the variable time step was adjusted as described in the overflow documentation.[5]

III. Results

A. Flat Plate

A Mach 5 flat plate[6] was simulated with baseline on a 129 × 129 grid(Fig. 2, with a Reynolds number based on (total)length of 10×10^6. The pressure wave created by the nose of the flat plate fits nicely within the grid, and wall spacing for this grid was constant at $\Delta y/L = 2 \times 10^{-6}$, which yeilded a $\Delta y^+ \approx 0.5$.

The inflow and external face boundary conditions were freestream (plug flow) at M=5 and $T_\infty = 273.15$, and the outflow boundary condition was simple extrapolation of all variables. Three cases were computed, one with an adiabatic wall by which the recovery factor of the model could be ascertained, and two fixed wall temperature cases, $T_w = 5.4T_\infty$ and $T_w = 2.7T_\infty$, one at roughly the adiabatic wall temperature and half that value.

The solution was also obtained on two coarser grids, a medium 65 × 65 grid obtained by removing every other point in both directions, and a coarse 33 × 33 grid again removing every other point, this time from the 65 × 65 grid. These grids have Δy^+ of approximately unity and two, respectively. The grid stretching ($\Delta x_{j+1}/\Delta x_j$) was less than 1.06 in the streamwise direction, and below 1.08 in the wall normal direction, for the finest grid. The medium (65 × 65) grid had stretching below 1.12 streamwise and 1.16 wall normal. The coarsest grid had stretching below 1.24 streamwise and 1.35 wall normal.

The Lag models skin friction predictions(here for the adiabatic wall) are in line with theoretical predic-

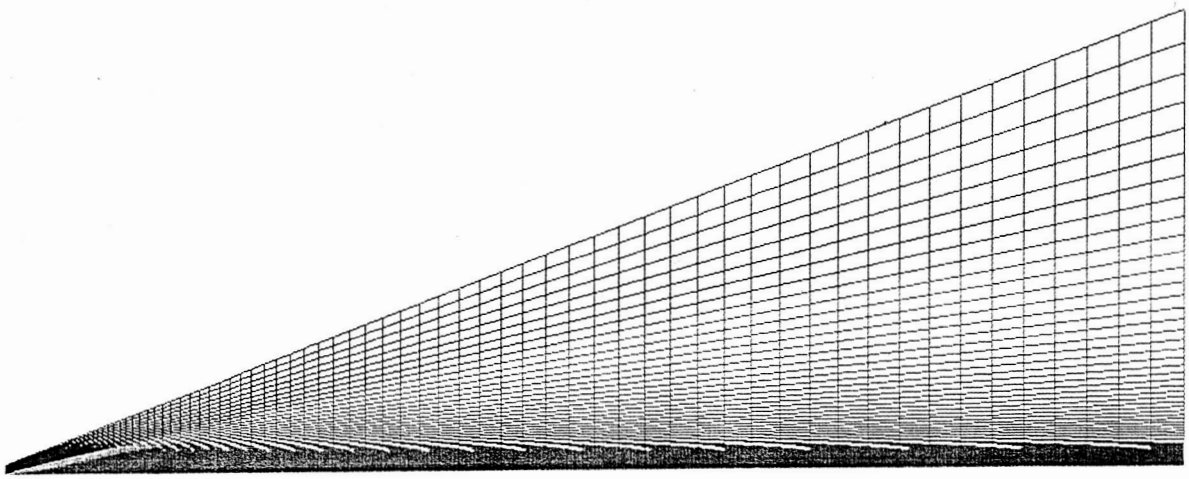

(a) Grid, Colored by Pressure

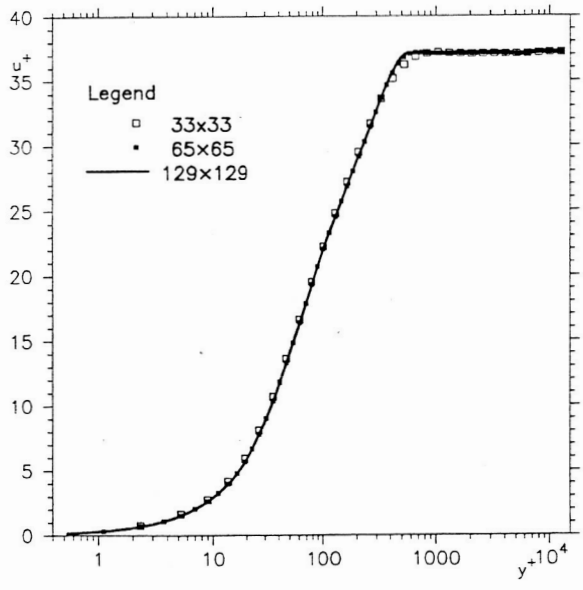

(b) Boundary Layer Grid Sensitivity

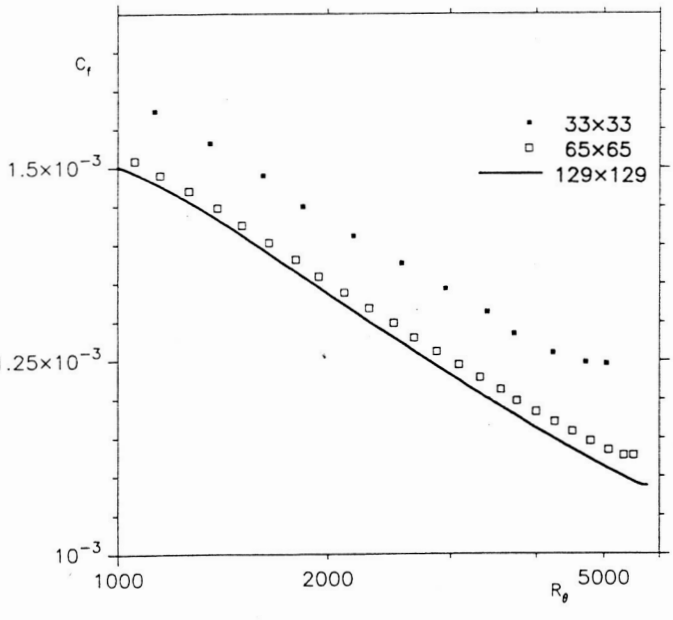

(c) c_f Grid Sensitivity

Figure 2. $M_\infty = 5$, $Re_L = 10 \times 10^6$ **Flat Plate**

tions(Van Driest II with Karman-Schoener), and with other turbulence models(Fig. ??). The model shows similar wall spacing dependence as for the subsonic flat plate, with the skin friction predictions (Fig. 2(c)) requiring a $\Delta y^+ \leq 1$ for accurate skin friction determination. The boundary layer predictions (here plotted in wall coordinates, Fig 2(b)), are insensitive to this variation in grid density. Another comparison to an essentially flat plate flow will be seen in the inflow profiles and upstream heat transfer reported below for the cylinder-flare flowfield.

Two skin friction predictions are shown for two wall temperatures, one essentially an adiabatic wall(Fig 3(a)), and the other a cold wall(Fig. 3(b)). Skin friction is well predicted in both cases. The heating rate for the cold wall is also well predicted(Fig 4(b)). The T_w predicted by the various turbulence models for adiabatic conditions varies slightly(Fig 4(a)), with the recovery factor of the SA[1] model at 0.89 and Lag, SST[7] and $k-\omega$[2] model at .895.

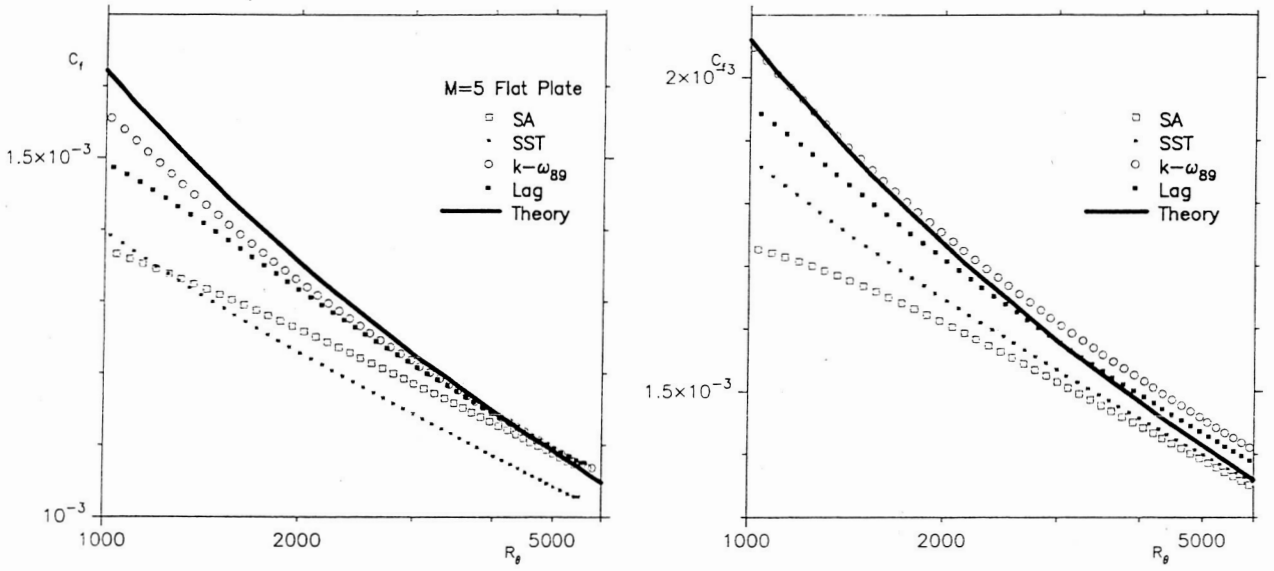

(a) c_f comparison, $T_w = 5.4T_t \approx T_{aw}$

(b) c_f comparison, $T_w = 2.7T_t \approx T_{aw}/2$

Figure 3. $M_\infty = 5$, $Re_L = 10 \times 10^6$ **Flat Plate Skin Friction**

B. Cylinder Flare

The $M_\infty = 7$ axisymmetric cylinder[8] flowfield tests the ability of the models to predict a simple well defined flowfield with a shock induced separation. The experimental geometries are an ogive-cylinder with cones of $20°, 30°, 32.5o$ and $35°$ attached 1.39m from the nose of the ogive-cylinder. The cylinder-cone intersection is chosen as the origin of the x axis. The ogive nose is described more fully in,[9] and consists of a $10°$ conical nose, with a circular blend to the constant diameter cylinder body 0.644m downstream of the nose($x = -0.746$m). The ogive nose was modelled in an effort to match the experimental conditions as closely as possible.

The finest grid for this case was 1179×257(streamwise×wall normal), extending from the ogive nose to the cylinder flare(Fig. 5). The interaction region 4mm ahead and behind the flare corner accounted for roughly 100 of the 1179 streamwise points. The portion upstream of this interaction region accounted for over 600 of the streamwise points, with the remaining points along the flare surface. Two sets of coarser grids were again created by removing every other point in both directions, resulting in a 589×129 and 295×65 grid systems. The wall normal spacing was varied along the cylinder-flare surface in order to keep the y^+ values within recommended values. This entailed very fine spacing along the face of the flare, 8 micron spacing in the region of the cylinder-flare intersection.

The velocity and thermal boundary layers were measured at a $x = -0.06$m (just upstream of the cylinder-cone corner). Transition was determined to be within the region $-1\text{m} \leq x_{tr} \leq -0.6\text{m}$, which includes a sizeable portion of the conical nose. Transition was set 0.8m upstream of the flare-cone intersection, and this choice did give the best match for the measured velocity and temperature boundary layers.

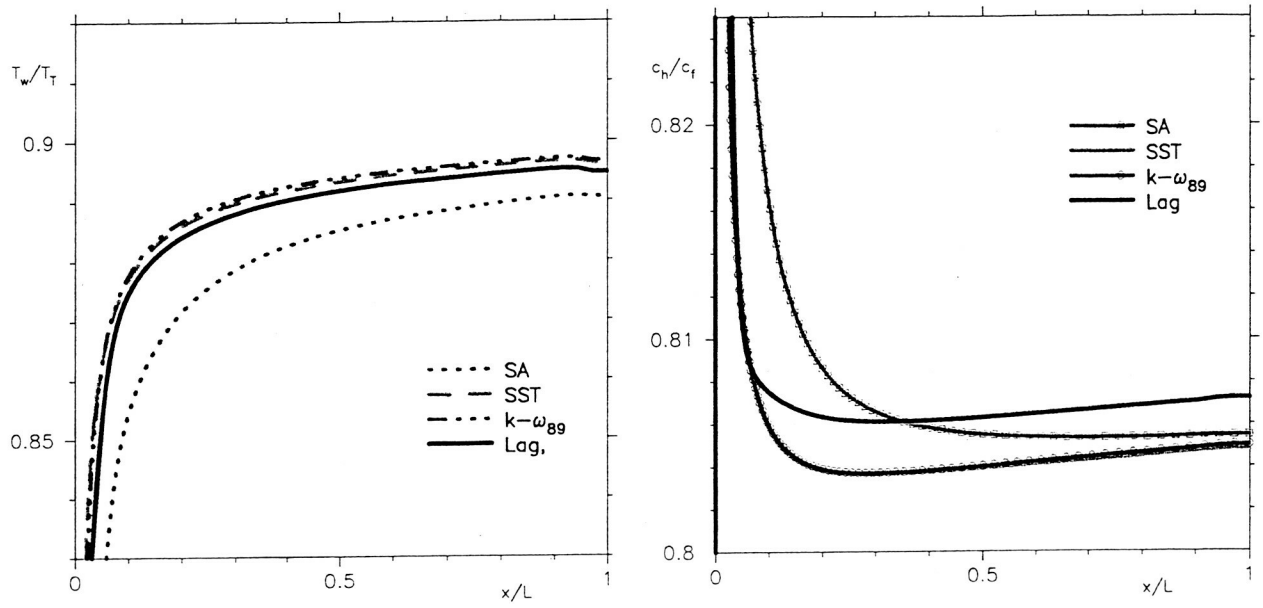

(a) Recovery Factor Prediction, Adiabatic Wall

(b) Heat Transfer Prediction, $T_w = .5T_{aw}$

Figure 4. $M_\infty = 5$, $Re_L = 10 \times 10^6$ **Flat Plate Heating**

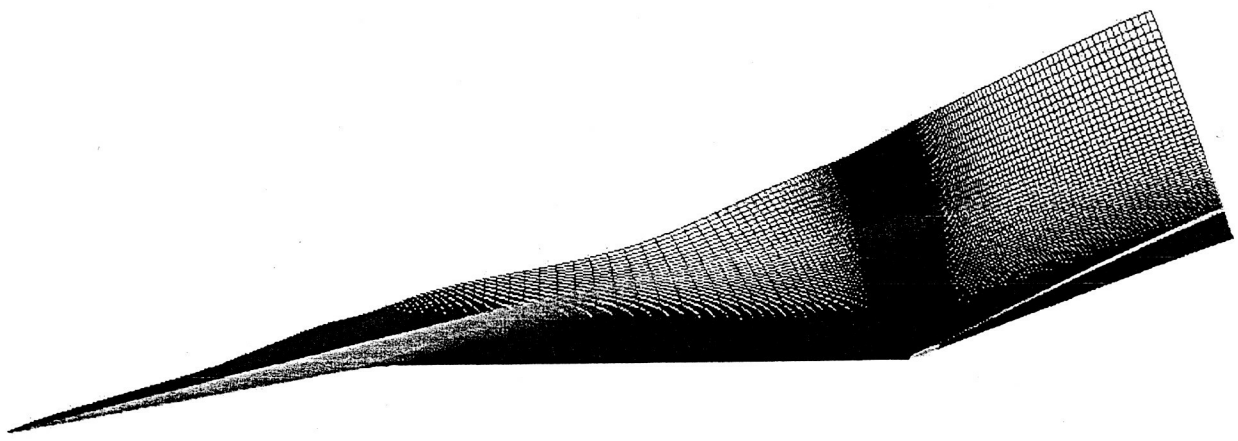

Figure 5. $M = 7$, 20° **Cylinder-Flare Grid Colored by Pressure**

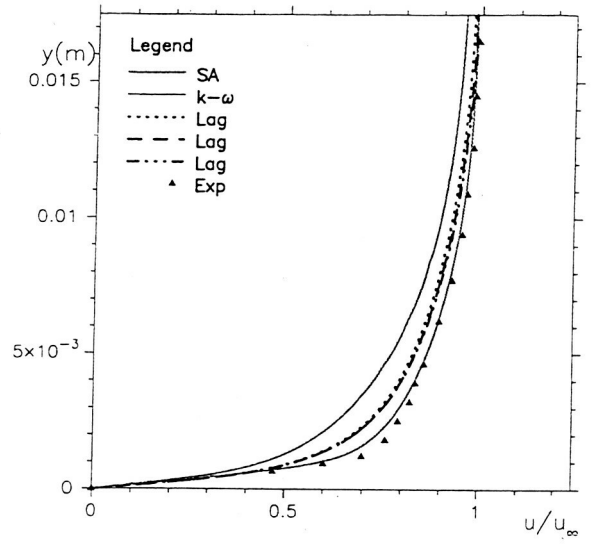

(a) Velocity Boundary Layer

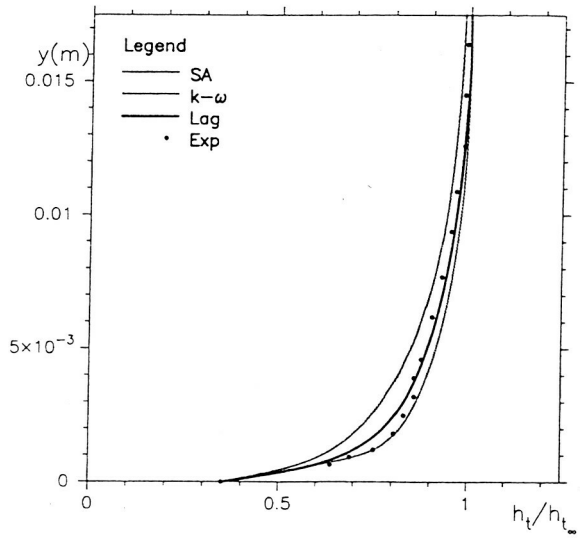

(b) Enthalpy Boundary Layer

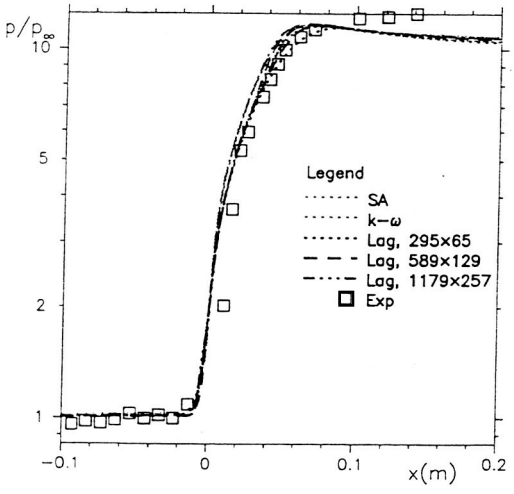

(c) p/p_∞, 20°

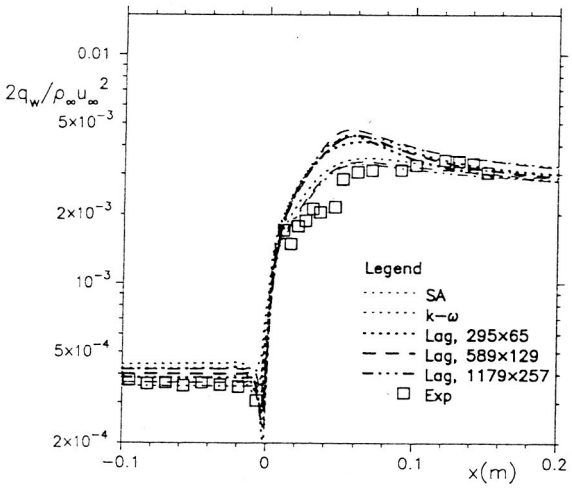

(d) Heat Transfer, 20°

Figure 6. Kussoy Cylinder Flare Upstream Boundary Layers, Pressure and Heat Transfer, $M_\infty = 7.05$, Attached Case

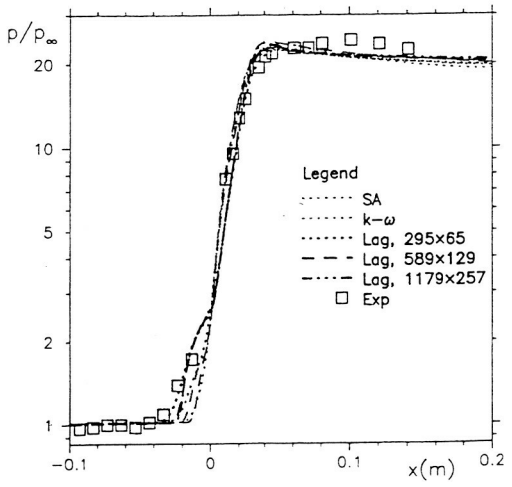

(a) p/p_∞, 30°

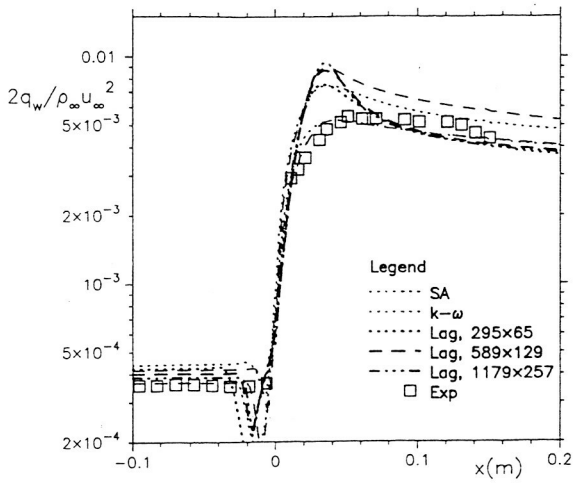

(b) Heat Transfer, 30°

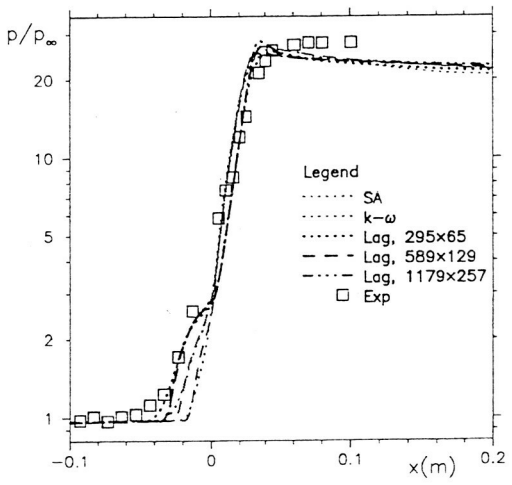

(c) p/p_∞, 32.5°

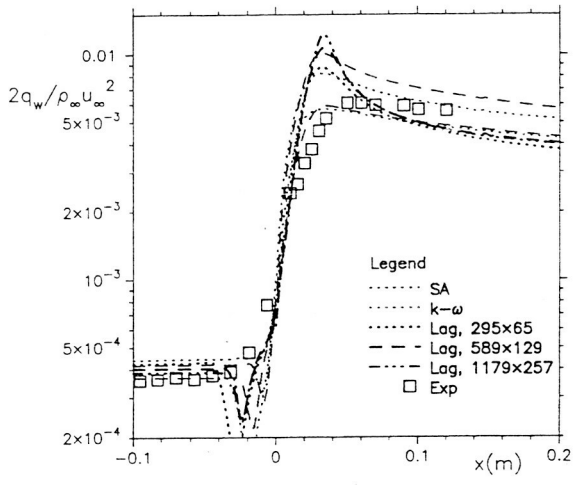

(d) Heat Transfer, 32.5°

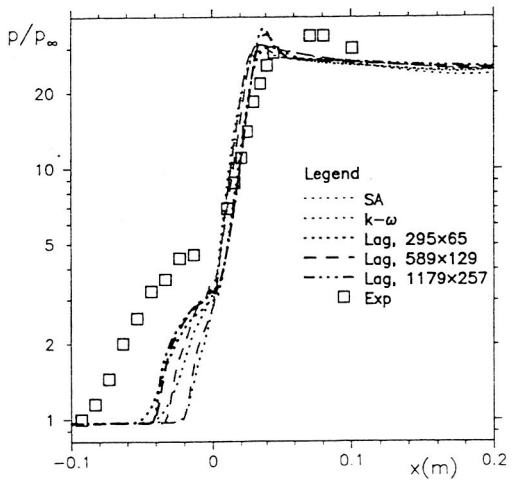

(e) p/p_∞, 35°

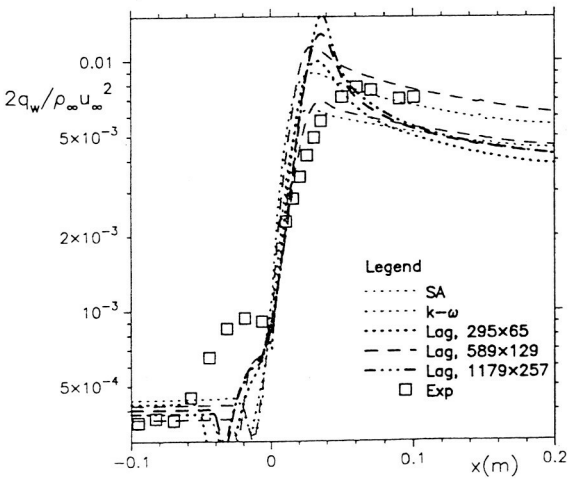

(f) Heat Transfer, 35°

Figure 7. Kussoy Cylinder Flare Pressure and Heat Transfer, $M_\infty = 7.05$, Separated Cases

The 20° case is attached flow. All the models predict pressure well for this case. The heat transfer predictions are less stellar, with all two equation models exhibiting a heat transfer peak not evident in the experimental results. The one equation models do not exhibit this overshoot, but underpredict the heating rate as the cone surface is downstream of the heating maximum where the other models better predict the heat transfer.

The 30° case is separated flow, The Lag model predicts the separation slightly better that SA, k-ω models, but all three are reasonable predictions. The SST model predicts a much larger separation than seen experimentally. The heat transfer predictions are in line with the 20° case, with no model performing flawlessly, although the SA model's predictions are argueably the best.

The 32.5° case has more separated flow than the 30° case., The SA, k-ω, and Lag models all predict pressure well for generally well for this case, with the Lag model again providing a slightly improved separation prediction. The SST models again gives an overprediction of the extent of the separation. The heat transfer predictions in again line with the 20° case, although the overshoot in heating is more pronounced.

The 35° case not predicted well by any of the models, The models all underpredict the extent of the separation, but SST gives the separation prediction closest to the experimental values. The heating rate predictions are even less satisfactory, as could be expected given the relatively poor separation predictions of the models.

Various compressibility corrections were attempted, but no universal corrections (in that they reproduced or improved earlier predictions, as well as improving these predictions) were found. This remains an ongoing area of research for this model.

C. Overexpanded Nozzle Flow

This flowfield is an important case for design and analysis of rocket motors utilized over a large range of external pressures, such as is the case for space launch vehicles. A 'cold flow'(non-reacting) rocket nozzle expands into an environment[10] with a backpressure sufficiently high to induce separation on the nozzle walls. This flowfield is simulated with the help of the chimera capabilities of OVERFLOW. The grid is composed of 5 zones: Nozzle Interior, Nozzle Lip, Nozzle Exterior, Near Field Downstream, and Farfield. The nozzle interior grid has dimentions 245 × 145, and comprises roughly 3/4 of all the points in the grid system.

The inflow boundary of the rocket nozzle is accomplished by combining two boundary conditions sequentially, a read of the full conservative conditions followed by a 'nozzle inflow' condition, which holds p_t and T_t constant, and zeros the radial and circumferential velocities. The static pressure and axial velocity are allowed to adjust. The walls are treated as adiabatic no slip surfaces, and the nozzle is immersed in a Freestream with $M_\infty = 0.2$, with characteristic boundary conditions.

Three cases are discussed in this paper, all involving separated flow in the nozzle interior. These cases are parameterized by the ratio of the rocket nozzle chamber pressure to the ambient farfield pressure(NPR).

The least separated flow discussed in this paper has a NPR of 66(Fig. 9(a)). For this case, all of the models predict the separation location adequately, and also do a reasonable job of prediction of the pressure in the separation region. The post separation presssure is reasonably well predicted.

A more seperated case has a NPR of 44(Fig. 9(b)), and has more extensive separation. For this case, the Lag model did not want to converge on a single location for the separation, and hence was then run in time accurate mode using dual timestepping. The time dependent process converged on a roughly constant separation/shock location, The range of the separation location for the relaxation includes the position predicted by the time accurate simulation. The time accurate solution did still exhibit some unsteadiness, and hence the 'steady state' solution for this case would be suspect in any event.

The SA, k-ω and SST models converged to a steady state solution without recourse to the time accurate simulation, but miss the separation location, and the pressure post separation. The k-ω model consistently underpredicts the separation extent, SST overpredicts the separation extent, and all three miss the post separation pressure level, which is more accurately predicted by the Lag model.

The final case has a NPR of 34(Fig. 9(c)), and the most extensive separation. Again, the Lag model did not want to converge on a single location for the separation, and hence was then run in time accurate mode using dual timestepping. The time dependent process again converged on a separation/shock location, though the variation of the shock location and post shock pressure were larger than exhibited by the previous case.

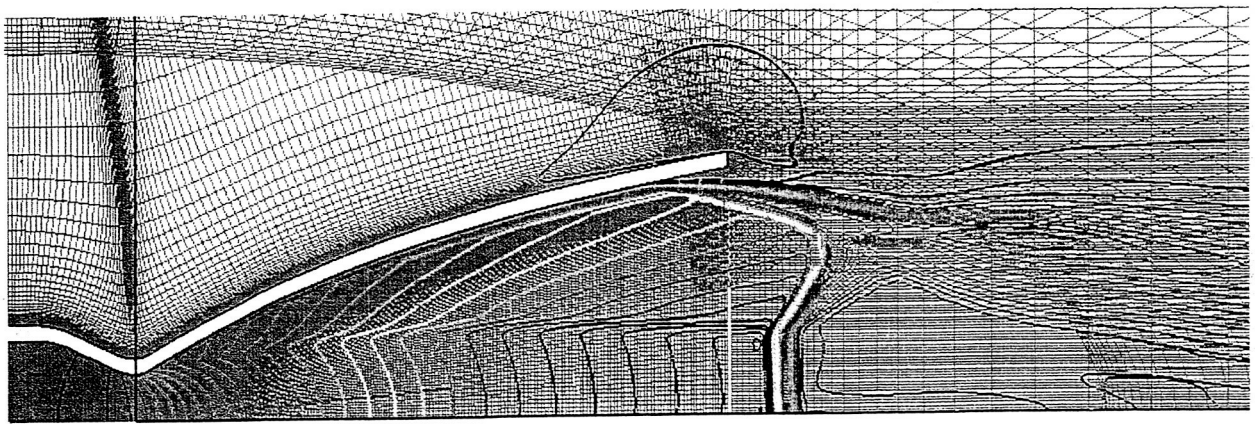

(a) NPR=66

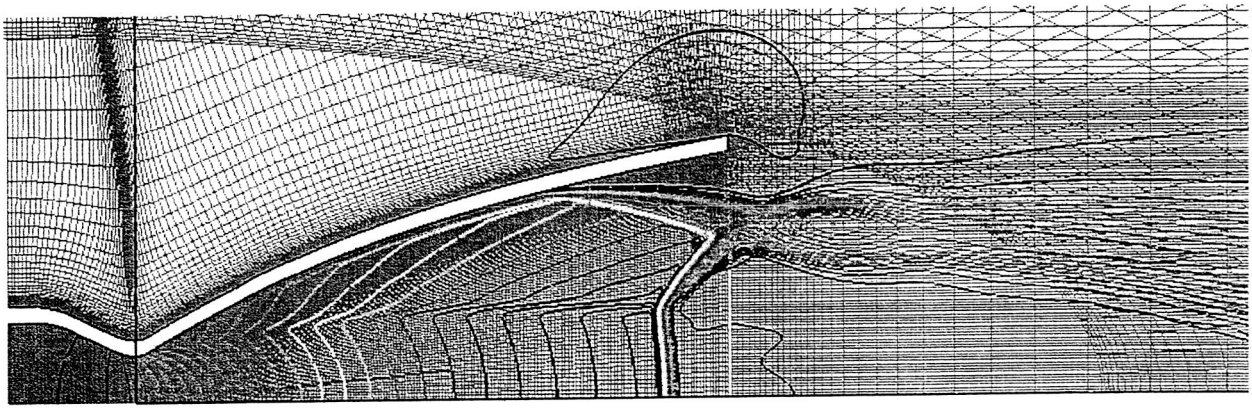

(b) NPR=44

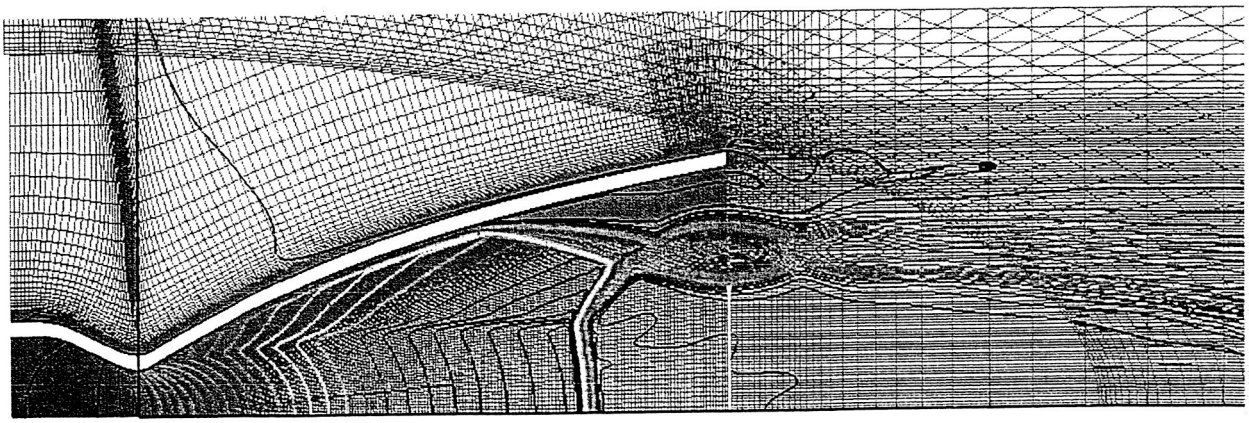

(c) NPR=34

Figure 8. Near Field Mach Number Contours, Lag Model

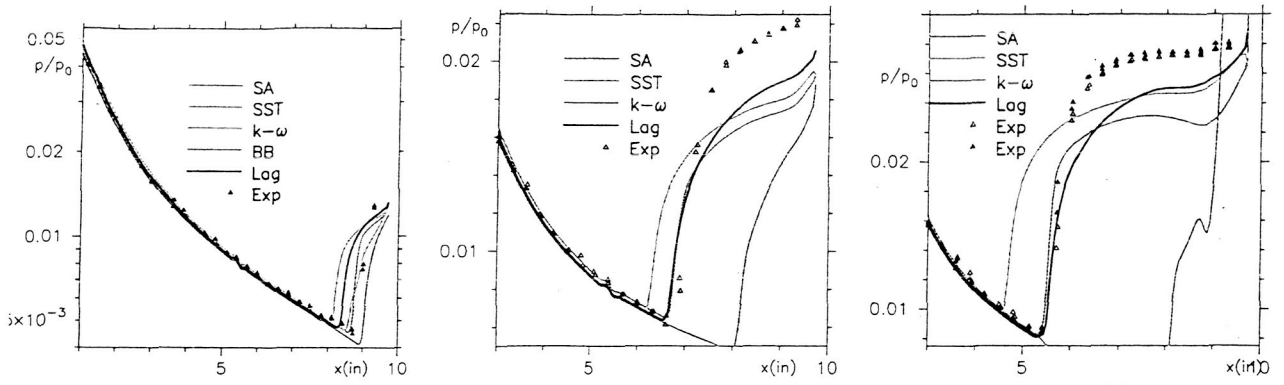

(a) NPR = 66 (b) NPR = 44 (c) NPR = 34

Figure 9. Nozzle Interior Wall Pressure Predictions for Various Backpressures.

D. Shuttle

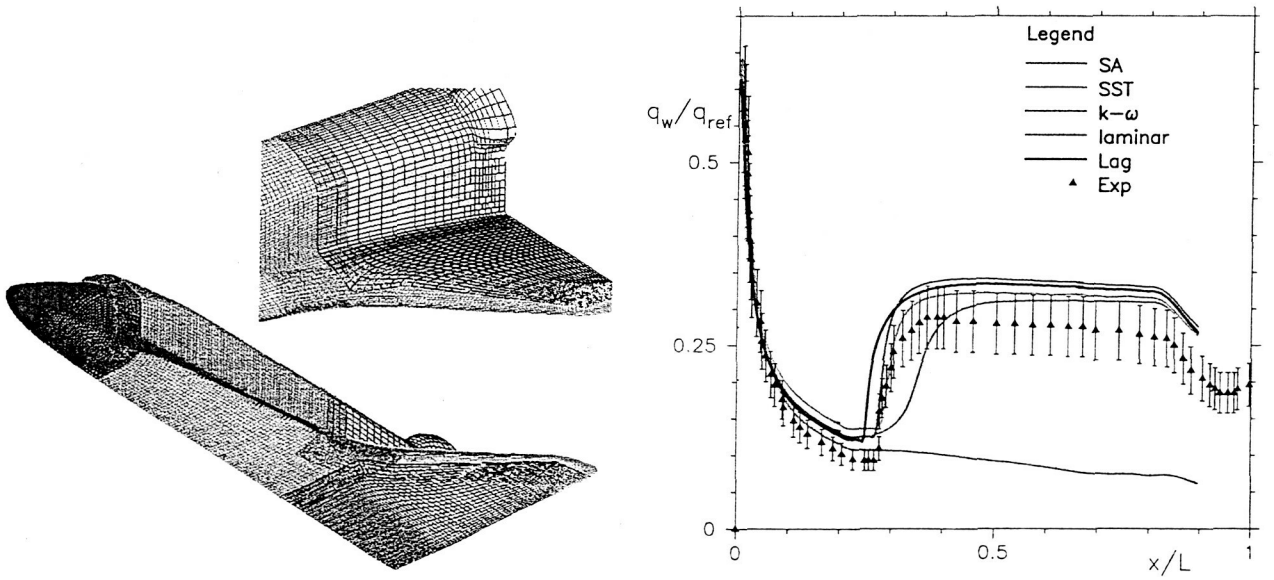

(a) Overset Grid System (b) Heating

Figure 10. Space Shuttle Orbiter, $M_\infty = 6.02$, $Re_L = 600 \times 10^3$, $\alpha = 40°$

After examining several axi-symmetric test cases, the lag model was applied to the Space Shuttle Orbiter at $M_\infty = 6.02$, $\alpha = 40°$. This configuration represents a complex geometric flowfield at a high angle of attack. Freestream conditions were $T_\infty = 62.31°K$, $p_\infty = 2032.2Pa$, $\rho_\infty = 0.1136kg/m^3$. The model length is .25m Wall conditions were modelled as a constant temperature ($T_w = 300°K$), no slip smooth wall. As this is attached flow, the most relevant comparison is the surface heating rate.

The shuttle data was obtained by Berry and Hamilton[11] in Langley's 20-inch Mach 6 wind tunnel.[12] It is a conventional blowdown facility with a 0.508 x 0.5207m rectangular test section. Electric heaters can vary the stagnation temperature up to 590K, and the normal operating stagnation pressure is approximately 7×10^5 to 3.7×10^6 Pa. Data was obtained by using phosphor thermography techniques. This method uses ceramic models that are coated with phosphors that when illuminated with ultraviolet light, fluoresce in two regions of the visible spectrum. The fluorescence intensity is dependent on the surface temperature. By taking fluorescence intensity images with a color video camera and calibrating the temperature prior to the

test, heat transfer can be calculated based on the surface temperature time histories. The thickness of the phosphor paint coating is approximately 0.001 inches thick.

The wind tunnel data was obtained in order to assess the effects of discrete roughness elements on transition. The trips were located at an X/L location of 0.258 This allowed for a majority of the windward surface to be turbulent. Computations were ran either fully turbulent or fully laminar.

Grid generation for the Shuttle Orbiter was based on the recommendations given by Chan et al[13] for overset grid generation. The orbiter was modelled using six zones. The grid for this case is pictured in Figure 10(a). The pitch plane of the orbiter was used as a symmetry plane with y-symmetry. Special care was take to ensure each grid had perpendicular grid lines to the pitch plane. Each grid extends from the surface to the outer boundary (upstream of the shock). A minimum of 5 grid points overlap between regions.

The outer boundary of each grid was fitted to the shock shape for the test condition. Stretching ratios are below 1.2 on the surface grids and in volume grids in the off-body direction. Volume grid generation took approximately one working day. The total number of grid points for the Shuttle Orbiter grid system was nearly 8 million with each grid having 85 points in the off-body direction. Wall spacing values were evaluated based on a Re_{cell} value given by Gnoffo.[14] $Re_{cell} = \frac{\rho_w a_w \Delta z}{\mu_w} \leq 1$ was maintained. The resulting y^+ values were on the order of 0.1 with the chosen wall spacings.

Heat transfer rates are compared in Figure 10(b). The laminar results compare within the experimental uncertainty until the flow was tripped, although they are consistently high. After approximately $X/L = 0.258$, the tripped flow became fully turbulent. All three turbulent predictions are higher than the experimental data, although the 2 equation model predictions are consistently higher than the SA model.

IV. Conclusions

The Lag model is a suitable model for computing high speed flows, including flows with separation. Skin friction is predicted predicted well for attached flowfields. Good separation predictions are obtained for both external and internal geometries. The prediction of the nozzle flow cases using a time accurate calculation is exciting. Heat transfer predictions need improvement for separated flows especially. The model has the advantages of not requiring wall distance, making it suitable for more advanced computational methods, and has shown some promise in computing separated flowfields when run in a time accurate mode.

References

[1] Spalart, P.R. and S.R. Allmaras. "A one equation Turbulence Model for Aerodynamic Flows". *La Recherche Aerospatiale*, 1:5–21, 1994.

[2] Wilcox, David C. . *"Turbulence Modeling for CFD"*. DCW Industries, Inc, 1993.

[3] Olsen, M.E. and Coakley T. J. " The Lag Model, a Turbulence Model for Non Equilibrium Flows". AIAA Paper 2003-2564, 2001.

[4] Olsen, Michael E. and Dinesh K. Prabhu. "Application of OVERFLOW to Hypersonic Perfect Gas Flowfields". AIAA Paper 2001-2664, 2001.

[5] Buning, Pieter G. et al. Overflow user's manual. Version 1.8, NASA Ames Research Center, February 1998.

[6] Bardina, J. E., Huang, P. G., and T.J. Coakley. "Turbulence Modeling Validation, Testing, and Development". NASA TM 110446, April 1997.

[7] Menter, F.R. "Two Equation Eddy Viscosity Model for Engineering Applications". *AIAA Journal*, 32:1299–1310, 1994.

[8] Kussoy, M.I. and Horstman, C.C. "Documentation of Two and Three-Dimensional Hypersonic Shock Wave/Turbulent Boundary Layer Interaction Flows". NASA TM 101075, January 1989.

[9] Kussoy, M.I. and Horstman, C.C. "An Experimental Documentation of a Hypersonic Shock-Wave Turbulent Boundary Layer Interaction Flow – with and without Separation". NASA TM X 62,412, February 1975.

[10] joseph.h.ruf@nasa.gov Joseph Ruf, Marshall Space Flight Center. Personal communication. 2004.

[11] Scott A. Berry and H. Harris Hamilton II. Discrete roughness effects on shuttle orbiter at mach 6. June 2002. AIAA 2002-2744.

[12] Charles G. Miller. Langley hypersonic aerodynamic/aerothermodynamic testing capabilities - present and future. June 1990. AIAA 90-1376.

[13] William M. Chan, Reynaldo J. Gomez, Stuart E. Rogers, and Pieter G. Buning. Best practices in overset grid generation. In *32nd AIAA Fluid Dynamics Conference, St. Louis, MO*, June 2002. AIAA 2002-3191.

[14] Peter A. Gnoffo, Roop N. Gupta, and Judy L. Shinn. Conservation Equations and Physical Models for Hypersonic Flows in Thermal and Chemical Nonequilibrium. Technical Report 2867, NASA Langley Research Center, Hampton, VA, February 1989.